A theoretical study of fragmentation dynamics of water dimer by proton impact

Zhi-Ping Wang(王志萍)[1,†], Xue-Fen Xu(许雪芬)[1], Feng-Shou Zhang(张丰收)[2], and Xu Wang(王旭)[1]

[1] *Department of Fundamental Courses, Wuxi Institute of Technology, Wuxi* 214121, *China*

[2] *The Key Laboratory of Beam Technology and Material Modification of Ministry of Education, College of Nuclear Science and Technology, Beijing Normal University, Beijing* 100875, *China*

(Received 9 May 2022; revised manuscript received 5 July 2022; accepted manuscript online 22 July 2022)

To investigate the collision processes of proton with the water dimer $(H_2O)_2$ at 50 eV, the time-dependent density functional theory coupled with molecular dynamics nonadiabatically is applied. Six specific collision orientations with various impact parameters are considered. The reaction channels, the mass distribution and the fragmentation mass spectrum are explored. Among all launched samples, the probability of the channel of non-charge transfer scattering and charge transfer scattering is about 80%, hinting that the probability of fragmentation is about 20%. The reaction channel of proton exchange process 2 is taken as an example to exhibit the detailed microscopic dynamics of the collision process by inspecting the positions, the respective distance, the number of loss of electrons and the evolution of the electron density. The study of the mass distribution and the fragmentation mass spectrum shows that among all possible fragments, the fragment with mass 36 has the highest relative abundance of 65%. The relative abundances of fragments with masses 1, 35, and 34 are 20%, 13%, and 1.5%, respectively. For the total electron capture cross section, the present calculations agree with the available measurements and calculations over the energy range from 50 eV to 12 keV.

Keywords: time-dependent density functional theory, water dimer, collision, proton

PACS: 34.50.Gb, 82.30.Fi, 36.40.Qv **DOI:** 10.1088/1674-1056/ac8340

1. Introduction

Collision-induced fragmentation of water by energetic projectiles has attracted extensive attention in biophysical and radiobiology research in the past decades.[1–7] This is mainly due to the fact that water molecules are the basic components of biological tissues and it has been found that irradiated water molecules usually produce a large number of secondary low-energy electrons, ions and radicals, which cause direct and indirect biological damage to DNA molecules through a series of chain reactions.[8–11]

As the hadron therapy has been applied mostly with proton beams, a variety of works dedicated to proton-water collisions experimentally[3,12–19] and theoretically.[20–32] These studies are helpful to understand the ionizing radiation of water impacted by protons. Water clusters are considered as transient intermediates in liquid water,[33] which is crucial to understand many chemical and physical processes.[34] Therefore, it is important to understand the interaction of protons with water clusters, which is directly relevant to a detailed understanding of radiation damage in biological systems. Although the water molecule has been the focus of scientific and technological research for many years, there is still no reasonable agreement among all reported measurements. Furthermore, the collision processes of water clusters impacted by low-energetic protons are relatively few in literature.

In this paper, we study the fragmentation dynamics of the water dimer in collision with 50 eV proton in the microscopic way using the approach of the time-dependent density functional theory (TDDFT) coupled to molecular dynamics (MD) non-adiabatically. The TDDFT-MD approach implemented in the code package PWTELEMAN developed by the Toulouse–Erlangen group[35–38] has been applied as an effective tool in exploring ion-molecule collision dynamics.[30–32,39–43]

The organization of this paper is as follows. In Section 2, we give a brief explanation of the theoretical and numerical approach. In Section 3, we discuss the calculated results. Finally, a summary is presented in Section 4.

2. Theory and simulation details

The system is treated as an ensemble composed of valence electrons and ions. The ions, which are composed of the inner shell electrons and their parent nuclei are treated as classical particles characterized by their positions $\boldsymbol{R}_I$, $(I = 1,\ldots,N_{\rm ion})$, where $N_{\rm ion}$ is the total number of ions. The valence electrons are described as single-particle wave functions $\varphi_j(\boldsymbol{r})$ $(j = 1,\ldots,N_{\rm el})$, where $N_{\rm el}$ is the total number of valence electrons. In the density functional theory (DFT), any observable could be written uniquely as a functional of the density of a non-interacting reference system.[44] The total energy of system is given as[36,37]

$$\begin{aligned} E_{\rm tot} &= E_{\rm kin,el}(\{\varphi_j\}) + E_{\rm C}(\rho) + E_{\rm xc}(\rho) + E_{\rm SIC}(\{|\varphi_j|^2\}) \\ &\quad + E_{\rm kin,ion}(\{\dot{\boldsymbol{R}}_I\}) + E_{\rm pot,ion}(\{\boldsymbol{R}_I\}) \end{aligned}$$

[†]Corresponding author. E-mail: zpwang03247@163.com

© 2023 Chinese Physical Society and IOP Publishing Ltd

$$+E_{\rm PsP}(\{\varphi_j\},\{\boldsymbol{R}_I\})+E_{\rm ext}, \tag{1}$$

where $\rho(\boldsymbol{r},t)$ is the electron density taking the form of $\rho(\boldsymbol{r},t)=\sum_j|\varphi_j(\boldsymbol{r},t)|^2$. In Eq. (1), $E_{\rm kin,el}$ is the electron kinetic energy, $E_{\rm C}$ denotes the direct Coulomb energy, $E_{\rm xc}$ represents the exchange-correlation energy and $E_{\rm SIC}$ is the self-interaction correction (SIC) term. $E_{\rm kin,ion}$, $E_{\rm pot,ion}$, $E_{\rm PsP}$ and $E_{\rm ext}$ denote the kinetic energies of ions, the ionic potential, the pseudo-potential and the external energy, respectively.

We perform real-time propagation of electron wave functions on the basis of time-dependent density functional theory (TDDFT). The time evolution of the electronic wave function is achieved by employing a set of time-dependent Kohn–Sham (TDKS) equations,[45] i.e.,

$$\mathrm{i}\frac{\partial}{\partial t}\varphi_j(\boldsymbol{r},t)=\left(-\frac{\nabla^2}{2}+V_{\rm eff}[\rho(\boldsymbol{r},t)]\right)\varphi_j(\boldsymbol{r},t), \tag{2}$$

with $V_{\rm eff}[\rho(\boldsymbol{r},t)]$ being the time-dependent Kohn–Sham potential,

$$\begin{aligned}V_{\rm eff}[\rho(\boldsymbol{r},t)] &= V_{\rm ne}(\boldsymbol{r},t)+V_{\rm H}[\rho(\boldsymbol{r},t)]\\ &\quad+V_{\rm xc}[\rho(\boldsymbol{r},t)]+V_{\rm ext}(\boldsymbol{r},t),\end{aligned} \tag{3}$$

where $V_{\rm ne}$ is the electron-ion potential, $V_{\rm H}$ is the Hartree potential, $V_{\rm xc}$ is the exchange–correlation (xc) potential, and $V_{\rm ext}(\boldsymbol{r},t)$ is the external potential.

The ion motion is obtained by using molecular dynamics (MD) simulations. The equations of motion can be obtained by variations of ionic position $\boldsymbol{R}_I$ and momentum $\boldsymbol{P}_I$, i.e.,

$$\frac{\partial}{\partial t}\boldsymbol{R}_I=\frac{\boldsymbol{P}_I}{M_I}, \tag{4}$$

$$\begin{aligned}\frac{\partial}{\partial t}\boldsymbol{P}_I &= -\nabla_{R_I}\left[\frac{1}{2}\sum_{I\neq J}\frac{Z_IZ_J}{|\boldsymbol{R}_I-\boldsymbol{R}_J|}\right.\\ &\quad\left.+\sum_{i=1}^{N_{\rm el}}\langle\varphi_j|V_{\rm PsP}(\boldsymbol{r}-\boldsymbol{R}_I)|\varphi_j\rangle+V_{\rm ext,ion}(\boldsymbol{R}_I,t)\right],\end{aligned} \tag{5}$$

where M_I and Z_I are the mass and charge of the ion number I. $V_{\rm PsP}$ and $V_{\rm ext,ion}$ represent the pseudo-potential and the interaction between ions and the external field, respectively.

The dynamical Eqs. (2)–(4) for electrons and ions are computed and solved simultaneously, and both electrons and ions are fully propagated in time. The coupling between electrons and ionic cores is mediated by Goedecker-type pseudopotentials.[46] The parameterization of Perdew and Wang[47] is applied for $E_{\rm xc}$. An average-density self-interaction correction (ADSIC)[48] is employed to put the single-particle energies at their correct values.

All calculations were performed on a 3D coordinate-space grid of $72\times72\times72$. The grid spacing is $0.412a_0$ in each direction. The damped gradient method[37] is applied to get the ground state wavefunctions of system. A constant time step for the propagation of the wave function and ionic motion is 0.000605 fs to ensure the numerical stability. The absorbing boundary condition is applied to avoid periodic reflecting electrons.[49]

To describe electronic excitation, the number of bound electrons $N(t)$, which associates with the time-dependent electronic density $\rho(\boldsymbol{r},t)$ within the finite volume V, is given as

$$N(t)=\int_V{\rm d}\boldsymbol{r}\rho(\boldsymbol{r},t). \tag{6}$$

Accordingly, the number of escaped electrons can be defined as $N_{\rm esc}(t)=N(t=0)-N(t)$.

It is known that the direct electron emission, i.e., free electrons released from bound states into the continuum, is less probable than the electrons captured by the proton at low energies.[39,40,50] As the incident energy of proton is 50 eV, this also holds for the present study. We concentrate on estimating the electron capture probabilities simply in the current work. When the proton approaches the water dimer, the electron capture (also called charge transfer) can be simply described as

$$p^+ + (\mathrm{H_2O})_2 \to p^q + \cdots, \tag{7}$$

where q denotes the final charge state of the proton.

The full space is divided into two regions: the analyzed box V and its complement $\bar{V}$. Thus, the many-body wave functions are separated into bound- and continuum-state parts respectively. The orbital-resolved bound probability $N_j(t)$ and continuum one $\bar{N}_j(t)$[49] at the evolving time t are given as

$$\begin{aligned}N_j(t) &= \int_V{\rm d}\boldsymbol{r}\rho_j(\boldsymbol{r},t)\\ &= \int_V{\rm d}\boldsymbol{r}|\varphi_j(\boldsymbol{r},t)|^2,\quad (j=1,\ldots,N_{\rm el}),\end{aligned} \tag{8}$$

$$\begin{aligned}\bar{N}_j(t) &= \int_{\bar{V}}{\rm d}\boldsymbol{r}\rho_j(\boldsymbol{r},t)\\ &= \int_{\bar{V}}{\rm d}\boldsymbol{r}|\varphi_j(\boldsymbol{r},t)|^2,\quad (j=1,\ldots,N_{\rm el}).\end{aligned} \tag{9}$$

The probability $P^{i+}(t)$, which is initially derived from the precise definition of multiple ionization probabilities through the full many-body wave functions,[49] is defined as

$$P^0(t)=N_1(t)\cdots N_{N_{\rm el}}(t), \tag{10}$$

$$P^{1+}(t)=\sum_{i=1}^{N_{\rm el}}N_1(t)\cdots\bar{N}_i(t)N_{N_{\rm el}}(t), \tag{11}$$

$$P^{2+}(t)=\sum_{i=1}^{N_{\rm el}-1}\sum_{j=2,j>i}^{N_{\rm el}}N_1(t)\cdots\bar{N}_i(t)\cdots\bar{N}_j(t)N_{N_{\rm el}}(t), \tag{12}$$

$$\vdots$$

$$P^{(N_{\rm el}-1)+}(t)=\sum_{i=1}^{N_{\rm el}}\bar{N}_1(t)\cdots N_i(t)\bar{N}_{N_{\rm el}}(t), \tag{13}$$

$$P^{N_{\rm el}+}(t)=\bar{N}_1(t)\cdots\bar{N}_{N_{\rm el}}(t). \tag{14}$$

The corresponding electron capture cross section is determined by

$$\sigma_{1,0} = 2\pi \int P^{1+}(b) b \mathrm{d}b, \tag{15}$$

$$\sigma_{1,-1} = 2\pi \int P^{2+}(b) b \mathrm{d}b, \tag{16}$$

where $\sigma_{1,0}$ and $\sigma_{1,-1}$ denote the single-electron capture and the two-electron capture cross section, respectively. The corresponding total electron capture cross section is calculated by

$$\sigma_{\mathrm{t}}^{\mathrm{cap}} = \sigma_{1,0} + 2\sigma_{1,-1}. \tag{17}$$

3. Results and discussion

The coordinate system for the projectile and the target molecule of the H^++$(H_2O)_2$ collision system is shown in Fig. 1. The water molecule playing as the proton donor lies in the xy plane and the hydrogen bond is along the x axis. The center of mass of the water dimer locates at the origin of a Cartesian coordinate system. The incident proton approaches the target from three different directions: (a) The proton moves along the x axis toward the negative side of the x axis and the impact parameter changes along the positive y (orientation I-1) and the negative y (orientation I-2). (b) The proton moves along the y axis toward the negative side of the y axis and b varies along the positive x (orientation Ⅱ-1) and the negative x (orientation Ⅱ-2). (c) The proton moves along the z axis toward the negative side of the z axis and the impact parameter varies along the positive x (orientation Ⅲ-1) and the negative x (orientation Ⅲ-2). In each orientation, the different impact parameters are taken into account. Here, $b = 0$–$5.0a_0$ with $\Delta b = 0.1a_0$ and $b = 5.2$–$8.0a_0$ with $\Delta b = 0.2a_0$. Totally, 390 collision samples are performed in the present work.

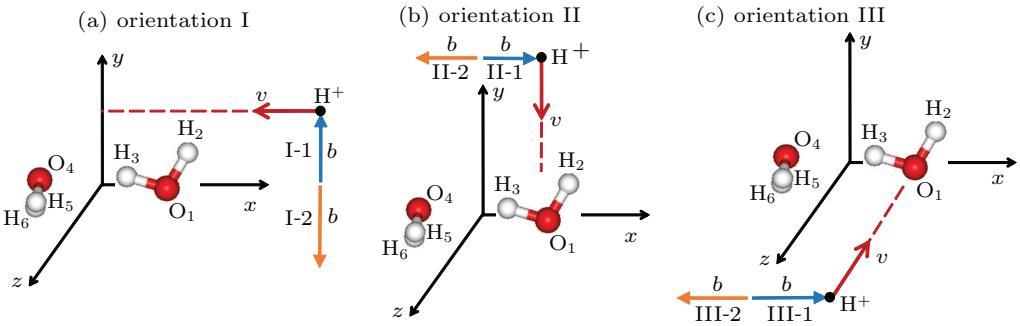


Fig. 1. Geometries of the H^++$(H_2O)_2$ collision system. Si_x target orientations are considered: (a) orientations I-1 and I-2, (b) orientations Ⅱ-1 and Ⅱ-2, (c) orientations Ⅲ-1 and Ⅲ-2. The black ball denotes the incident proton. Red arrows point out the incident direction, and the impact parameter is denoted by b.

3.1. Dynamical process

Here, we discuss the collision dynamical processes characterized by chemical reactive channels. By observing the nuclear separation carefully, we analyze the reaction type simply as the proton moves far enough away from the target. The obtained specific reaction channels are given as follows:

(a) Non-charge transfer (NCT) scattering: a collision between the proton and valence electrons, while the energy of proton transferred to the valence electrons is less than the minimum excitation energy of valence electrons:

$$\mathrm{p}^+ + (\mathrm{H_2O})_2 \rightarrow \mathrm{p}^+ + (\mathrm{H_2O})_2. \tag{18}$$

(b) Charge transfer (CT) scattering: a collision between the proton and valence electrons, while the energy of the proton transferred to the valence electrons is more than the minimum excitation energy of valence electrons:

$$\mathrm{p}^+ + (\mathrm{H_2O})_2 \rightarrow \mathrm{p}^{q_1} + [(\mathrm{H_2O})_2]^{q_2} + (N_{\mathrm{esc}})\,\mathrm{e}^-,$$
$$q_1 + q_2 = +(1 + N_{\mathrm{esc}}). \tag{19}$$

(c) Proton exchange process 1 (PE1): a collision between the proton and nuclei, while the proton exchanges the H atom in water dimer and a new water dimer is formed:

$$\mathrm{p}^+ + (\mathrm{H_2O})_2 \rightarrow \mathrm{H}^{q_1} + (\mathrm{H_3O_2p})^{q_2} + (N_{\mathrm{esc}})\,\mathrm{e}^-,$$
$$q_1 + q_2 = +(1 + N_{\mathrm{esc}}). \tag{20}$$

(d) Proton exchange process 2 (PE2): a collision between the proton and nuclei, while the proton exchanges the H atom in water dimer and two isolate H atoms split from the dimer:

$$\mathrm{p}^+ + (\mathrm{H_2O})_2 \rightarrow \mathrm{H}^{q_1} + \mathrm{H}^{q_2} + (\mathrm{H_2O_2p})^{q_3} + (N_{\mathrm{esc}})\,\mathrm{e}^-,$$
$$q_1 + q_2 + q_3 = +(1 + N_{\mathrm{esc}}). \tag{21}$$

(e) Proton exchange process 3 (PE3): a collision between the proton and nuclei, while the proton exchanges the H atom in water dimer and three isolate H atoms split from the dimer:

$$\mathrm{p}^+ + (\mathrm{H_2O})_2 \rightarrow \mathrm{H}^{q_1} + \mathrm{H}^{q_2} + \mathrm{H}^{q_3} + (\mathrm{HO_2p})^{q_4} + (N_{\mathrm{esc}})\,\mathrm{e}^-,$$
$$q_1 + q_2 + q_3 + q_4 = +(1 + N_{\mathrm{esc}}). \tag{22}$$

(f) Collision-induced O–H dissociation 1 (O–H DIS1): a collision between the proton and nuclei, while the H atom in water dimer is scattered by proton and an isolate OH radical is formed as well as an isolate H_2O:

$$\mathrm{p}^+ + (\mathrm{H_2O})_2 \rightarrow \mathrm{p}^{q_1} + \mathrm{H}^{q_2} + (\mathrm{OH})^{q_3} + (\mathrm{H_2O})^{q_4} + (N_{\mathrm{esc}})\,\mathrm{e}^-,$$
$$q_1 + q_2 + q_3 + q_4 = +(1 + N_{\mathrm{esc}}). \tag{23}$$

(g) Collision-induced O–H dissociation 2 (O–H DIS2): a collision between the proton and nuclei, while the H atom in water dimer is scattered by proton and a radical H_3O_2 is formed:

$$\begin{aligned} &p^+ + (H_2O)_2 \rightarrow p^{q_1} + H^{q_2} + (H_3O_2)^{q_3} + (N_{esc})\,e^-, \\ &q_1 + q_2 + q_3 = +(1 + N_{esc}). \end{aligned} \tag{24}$$

(h) Collision-induced O–H dissociation 3 (O–H DIS3): a collision between the proton and nuclei, while two H atoms in one water molecule is scattered:

$$\begin{aligned} &p^+ + (H_2O)_2 \rightarrow p^{q_1} + H^{q_2} + H^{q_3} + (H_2O_2)^{q_4} + (N_{esc})\,e^-, \\ &q_1 + q_2 + q_3 + q_4 = +(1 + N_{esc}). \end{aligned} \tag{25}$$

(i) Collision-induced O–H dissociation 4 (O–H DIS4): a collision between the proton and nuclei, three H atoms split from the water dimer:

$$\begin{aligned} &p^+ + (H_2O)_2 \rightarrow p^{q_1} + H^{q_2} + H^{q_3} + H^{q_4} \\ &+ (O_2H)^{q_5} + (N_{esc})\,e^-, \\ &q_1 + q_2 + q_3 + q_4 + q_5 = +(1 + N_{esc}). \end{aligned} \tag{26}$$

(j) Collision-induced O–H dissociation 5 (O–H DIS5): a collision between the proton and nuclei, four H atoms split from the water dimer:

$$\begin{aligned} &p^+ + (H_2O)_2 \rightarrow p^{q_1} + H^{q_2} + H^{q_3} + H^{q_4} + H^{q_5} \\ &+ (O_2)^{q_6} + (N_{esc})\,e^-, \\ &q_1 + q_2 + q_3 + q_4 + q_5 + q_6 = +(1 + N_{esc}), \end{aligned} \tag{27}$$

where q_1, q_2, q_3, q_4, q_5 and q_6 represent the charge states of ions.

All of the possible reaction channels are enumerated in Table 1. One can find that different orientations lead to different reaction channels. In the orientations I-1 and Ⅱ-1, there are more kinds of reaction channels and abundant products than in other cases. Furthermore, one can find that the reaction channel shows the discrete diversity even if the impact parameter changes little. One of the reasons for this phenomenon is that the low-energy collisions are more sensitive to the electron density distribution. It is known that there are two counteracting influences on the collision process. On the one hand, the faster proton exposes higher frequency components to water dimer. On the other hand, the slower proton lengthens the interaction time, which leads to an enhanced reaction yield in turn. In the present simulation, reliable pseudopotentials were employed to treat the interaction between active electrons and ionic cores, and the Ehrenfest method was used to couple electronic and ionic motions self-consistently at each evolution time step. Since the time-dependent density functional theory (TDDFT) is coupled to molecular dynamics non-adiabatically, as the impact parameter changes little, the reaction process is affected sensitively. PE1 occurs in the cases of I-1 at $b = 1.5a_0$ and Ⅱ-2 at $b = 1.8a_0$. PE2 and PE3 appear in the orientation Ⅱ-1 at $b = 2.3a_0$ and $b = 0.8a_0$, respectively. Among all 390 samples, the probability of the channel of NCT and CT is about 80%. In addition, the probabilities of O–H DIS2 and O–H DIS3 are 15.6% and 1.8%, respectively.

Table 1. The reaction channels of the water dimer impacted by 50 eV proton in six orientations.

Incident configuration	Impact parameter (a_0)	Reaction process
I-1	0.3,0.5	O–H DIS1
	0.6–1.2,1.7–1.8	O–H DIS2
	0.2,0.4,1.4,1.6	O–H DIS3
	1.3	O–H DIS4
	1.5	PE1
	0.1,1.9–8.0	NCT and CT
I-2	0.2–0.4	O–H DIS2
	0.1,0.5–8.0	NCT and CT
Ⅱ-1	0.4–0.5,0.9–1.1,1.3–1.5,2.2,2.4,3.3–3.5,3.7–4	O–H DIS2
	1.2,1.6,3.6	O–H DIS3
	0.7	O–H DIS4
	0.6	O–H DIS5
	2.3	PE2
	0.8	PE3
	0.1–0.3,1.7–2.1,2.5–3.2,4.1–8.0	NCT and CT
Ⅱ-2	1.9	O–H DIS2
	1.8	PE1
	0.1–1.7,2.0–8.0	NCT and CT
Ⅲ-1	0.5-3.5	O–H DIS2
	0.1–0.4,3.6–8.0	NCT and CT
Ⅲ-2	2.3–2.4	O–H DIS2
	0.1–2.2,2.5–8.0	NCT and CT

The process of PE2 taking place in orientation Ⅱ-1 at $b = 2.3a_0$ is taken as an example for exploring the fragmentation dynamics in detail. Figure 2(a) shows the positions of ions of the water dimer and the proton in the y axis as a function of time. The inset in Fig. 2(a) gives the scattering trajectories of proton (red circle), O_1 (black circle), H_3 (green circle), and H_6 (navy circle) in the xy plane. The arrows indicate the trends of ionic trajectories over time. It is obvious from Fig. 2(a) that the proton (red dashed line) approaches the water dimer along the negative direction of the y axis. At about 6.7 fs, the proton is closest to O_1. It is replaced with H_3 immediately. H_3 (green solid line) gains the kinetic energy from the proton and departs from the target quickly. H_6 (navy solid line) is hit by H_3 at about 10.3 fs. Obviously, the inset in Fig. 2(a) shows that this is a chain reaction. Eventually, both H_3 and H_6 leave away, while the proton stays with the remaining part of the water dimer.

Figure 2(b) gives the time evolution of the relative distances between ions. The distances O_1H_3 (cyan dashed line) and O_4H_6 (magenta dashed dot line) increase rapidly from about 7 fs and 9.8 fs, respectively. The distance O_4H_3, i.e., the length of the hydrogen bond (blue solid line), decreases first and attains a minimum $1.1a_0$ at about 9.2 fs. Then it increases immediately as H_3 is hit by the proton. The rapid increases of O_1H_3, O_4H_6 and O_4H_3 indicate that they are all broken. The distance between O_1 and the proton (olive solid line) reaches a minimum $1.9a_0$ at about 6.7 fs. Then it makes two cycles of the stretching vibration (the estimated frequency is about 2750 cm^{-1}), informing that a new OH bond is formed between the proton and O_1. However, it is only a temporary OH bond by observing the subsequent irregular vibration. Keep an eye on the proton, it is easy to find that it forms a stable OH bond with O_4 from about 54 fs. The new formed OH bond maintains a stable vibration with a bond length equivalent to that of O_4H_5 (red dot line) and a frequency of about 2500 cm^{-1}. Two OH bonds, i.e., O_1H_2 (black solid line) and O_4H_5 (red dot line) remain vibrating after the collision. The estimated vibration frequency of O_1H_2 is about 2730 cm^{-1}. In addition, the distance O_1O_4 (dark yellow solid line) is always less than the initial value throughout the process. The above results show that a stable O_2H_2p, that is, a new O_2H_3 is formed.

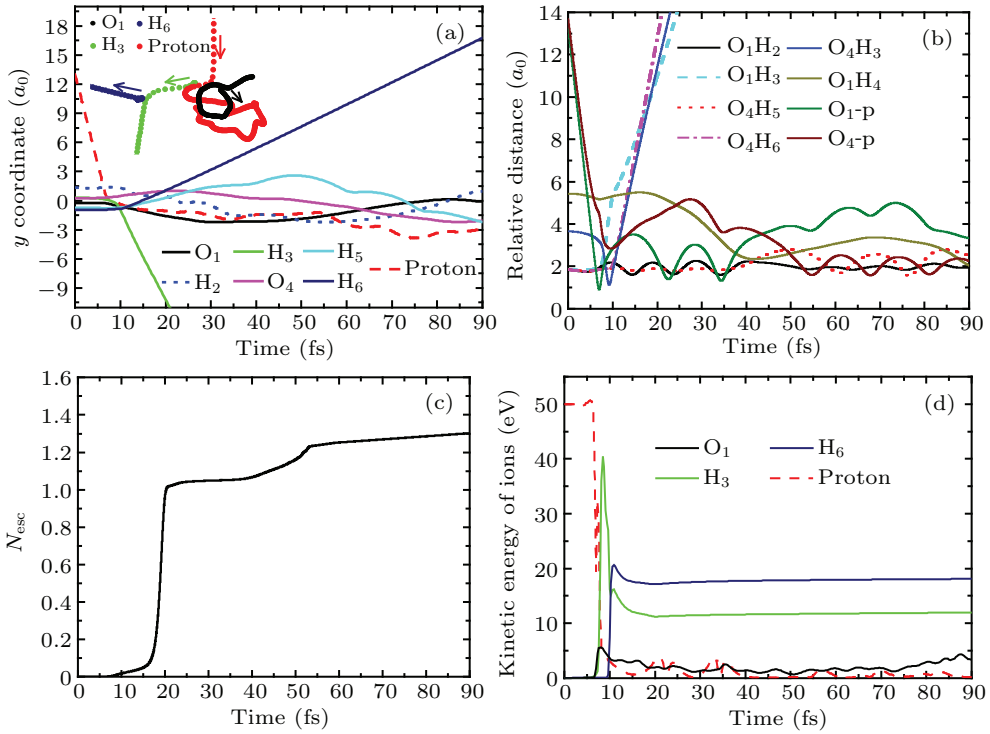


Fig. 2. The process of PE2 in orientation Ⅱ-1 at $b = 2.3a_0$. (a) The time evolution of positions of ions of the water dimer and the proton in the y axis. (b) The relative distances between ions as a function of time. (c) The time evolution of the loss of electrons of the water dimer. (d) The kinetic energies of proton, H_3 and H_6, versus time.

For electrons, it is obvious in Fig. 2(c) that N_{esc} starts to increase slowly from about 6.7 fs. From about 17 fs to 22 fs, it increases rapidly from about 0.06 to 1.03. This is mainly due to the fact that H_3 and its surrounding electrons depart from the target molecule quickly to the calculation boundary resulting the absorption of electrons around H_3 by the absorption boundary. From about 37 fs, N_{esc} increases slowly again until 55 fs because of the department of H_6. In this stage, about 0.2 electrons are lost, implying that H_6 takes away 0.2 electrons.

Figure 2(d) represents the kinetic energies of the proton, H_3 and H_6, versus time. The kinetic energy of proton (red dashed line) shows a small protrusion at around 4.5 fs. It decreases rapidly to 20 eV at about 5.7 fs, then increases quickly to 32.5 eV, and then decreases rapidly again to 5.5 eV. The re-

peated decrease and increase of the proton kinetic energy are caused by the medium-range polarization interaction. After the closest approach, the kinetic energy of proton is less than 3.8 eV in the remaining time. Finally, the proton loses about 46.2 eV of the kinetic energy, that is, 92% of the incident kinetic energy. The kinetic energies of H_3 (green solid line) and H_6 (navy solid line) exhibit the same trend as that of the proton and attain about 11.4 eV and 17.4 eV, respectively. The kinetic energy of O_1 (black solid line) starts to increase quickly at around 6.7 fs attaining 5.6 eV within 1 fs. It changes slightly and remains less than 5.6 eV in the remaining time.

Figure 3 represents six snapshots of the evolving process of the water dimer impacted by the proton in the same case as in Fig. 2. The proton approaches the water dimer gradually along the negative direction of the y axis ($t = 3.025$ fs, 6.05fs). When $t = 9.075$ fs, the proton is between two oxygen ions acting as a bridge. At $t = 18.15$ fs, H_3 and H_6 are far away from the target molecule. It can be seen that H_3 carries some electrons (about one electron). In the remaining time, the rest of the target molecule forms a stable structure H_2O_2p with the proton ($t = 45.375$ fs, 87.725 fs).

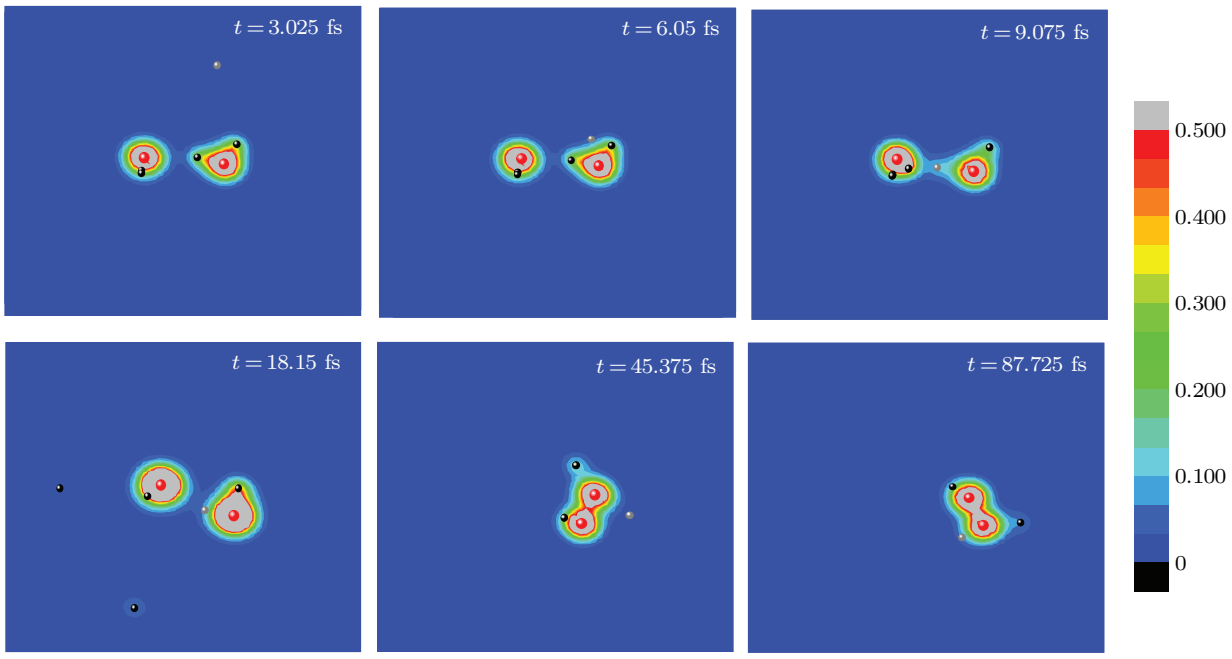


Fig. 3. Six snapshots of the evolving process of the water dimer impacted by the proton in the same case as in Fig. 2. Full red and black circles are oxygen ions and hydrogen ions. The proton is presented by grey circles. The observer sees the three-dimensional snapshots from the z axis. The simulation time is appended in the figures.

In short, the above case exhibits the detailed microscopic dynamics of the collision process from the perspectives of both electrons and ions. In the reaction channel of PE2, the proton replaces one hydrogen ion in the water dimer. At the same time, due to the chain collision reaction, two hydrogen ions on the water dimer separate from the target molecule. Finally, the target molecule and proton form a stable H_2O_2p structure.

Through the analysis of the reaction channels in Table 1, Fig. 4(a) shows the mass distribution of the fragments of the water dimer in each orientation. The masses of fragments are distinguished from the final products produced by various reaction channels. According to Table 1, there are eight kinds of the mass of the fragments: 1, 17, 18, 32, 33, 34, 35, and 36. Here, 36 refers to the parent peak. The fragment mass 1 counts 23, 32, and 32 in orientation I-1, Ⅱ-1, and Ⅲ-1, respectively, which is much higher than than that in other three cases (3 counts in case I-2, 2 counts in case Ⅱ-2, and 2 counts in case Ⅲ-2). Accordingly, mass 35 is 9, 18 and 31 in case I-1, Ⅱ-1 and Ⅲ-1, respectively, which is also higher than that in other three cases (3 counts in I-2, 1 count in Ⅱ-2, and 2 counts in Ⅲ-2). In each orientation, the count of the mass 36 is the largest compared with those of the other fragment masses. Furthermore, the mass 36 reaches 64 counts in both cases Ⅱ-2 and Ⅲ-2. For case I-1, the water dimer has the most abundant products after collision. There are seven kinds of fragments, including the fragment masses of 17 (2 counts) and 18 (2 counts), the mass 33 (1 count), the mass 34 (4 counts), the mass 35 (9 counts), and the mass 36 (49 counts). Figure 4(b) shows the fragmentation mass spectrum of the water dimer. The y axis represents the relative abundances of various fragments, that is, the percentage of the occurrence of various fragments in the total occurrence of fragments. In order to show clearly, the abundances of mass 17, mass 18, mass 32, and mass 33 are expanded by three times, respectively. The appearance probability of the mass 36 is about 65%, which is the highest. The probabilities of the fragment mass 1, mass 35, and mass 34 are 20%, 13%, and 1.5%, respectively. The probabilities of mass 17, mass 18, mass 32, and mass 33 are all less than 0.4%.

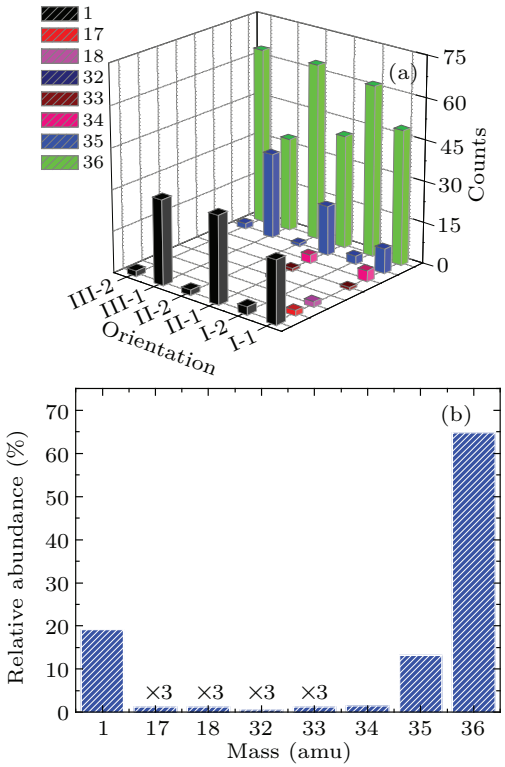


Fig. 4. (a) The mass distribution of the fragments of the water dimer impacted by the 50 eV proton in six orientations. (b) Fragmentation mass spectrum of the water dimer after collisions with the 50 eV proton.

The calculated single-electron capture cross section $\sigma_{1,0}$, the two-electron capture cross section $\sigma_{1,-1}$, and the total electron capture cross section σ_t^{cap} in each orientation are listed in Table 2. It is obvious that the single-electron capture cross section is larger than the two-electron capture cross section in each orientation. The total electron capture cross sections in all orientations are different from each other. Furthermore, the orientation Ⅱ-1 shows the largest cross sections of $\sigma_{1,0}$ and $\sigma_{1,-1}$. The averaged electron capture cross sections over all orientations are $\bar{\sigma}_{1,0} = 14.27 \times 10^{-16}$ cm^2, $\bar{\sigma}_{1,-1} = 2.56 \times 10^{-16}$ cm^2, and $\bar{\sigma}_t^{cap} = 19.40 \times 10^{-16}$ cm^2, respectively. The calculated total electron capture cross section of the water dimer impacted by 50 eV proton is 1.72×10^{-16} cm^2 higher than that of the water dimer attacked by the 250 eV proton.[51] Up to date, to the best of our knowledge, the experimental data of collision between the 50 eV proton and the water dimer is unavailable. Therefore, the direct comparison of the present calculations with experimental data could not be performed. In literature, the ionization cross section for the production of positive ions from H_2O by 50 eV electron impact measured by Rao *et al.* is about 2.76×10^{-16} cm^2,[52] and the cross sections for one-electron capture by He^{2+} ions in H_2O leading to He^+ formation measured using the TES technique are about 1.4×10^{-16} cm^2.[5] Therefore, one can conclude that the calculated total electron capture cross section of the water dimer impacted by the 50 eV proton is about one order of magnitude larger than that of water molecules collided by electrons and by He^{2+} with the same incident energy.

Table 2. The calculated electron capture cross sections σ ($\times 10^{-16}$ cm^2) in six orientations, i.e., $\sigma_{1,0}$: the single-electron capture cross section, $\sigma_{1,-1}$: the two-electron capture cross section, σ_t^{cap}: the total electron capture cross section.

Incident orientation	$\sigma_{1,0}$	$\sigma_{1,-1}$	σ_t^{cap}
I-1	11.34	1.76	14.86
I-2	12.34	1.93	16.20
Ⅱ-1	16.04	3.47	22.98
Ⅱ-2	15.73	2.65	21.03
Ⅲ-1	14.46	3.03	20.52
Ⅲ-2	15.72	2.53	20.78

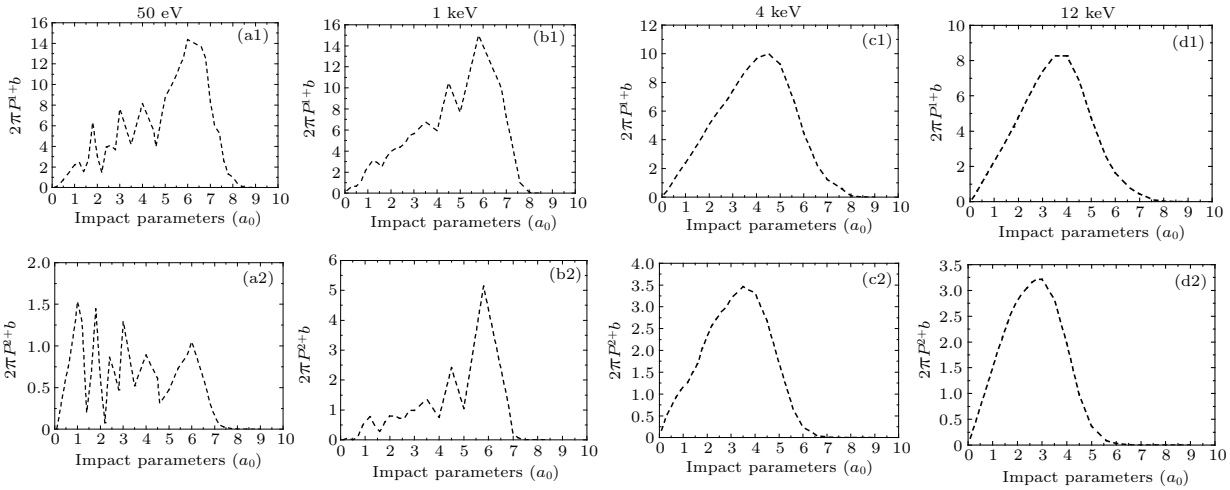


Fig. 5. Electron capture probabilities ($2\pi P^{n+}b$; $n = 1$ and 2 represent single- and two-electron capture, respectively) as a function of the impact parameters at an incident energy of 50 eV, 1 keV, 4 keV, and 12 keV, respectively. The first line is for $2\pi P^{1+}b$ and the second line is for $2\pi P^{2+}b$.

In Fig. 5, the averaged single- and two-electron capture probabilities $2\pi P^{n+}b$ ($n = 1, 2$) are exhibited for four incident energies: 50 eV, 1 keV, 4 keV, and 12 keV. It is obvious that the electron capture probabilities show large differences as the incident energy varies from 50 eV to 12 keV. With regard to the single- and two-electron capture probabilities for the same incident energy, we note that $2\pi P^{1+}b$ is higher than $2\pi P^{2+}b$. The probability lines of 4 keV [Figs. 5(c1) and 5(c2)] are simi-

lar to those of 12 keV [Figs. 5(d1) and 5(d2)]. However, as the impact energy decreases, the probability curves become divergent. At the low incident energy of 50 eV, the probability lines [Figs. 5(a1) and 5(a2)] are divergent, implying that low-energy collisions are more sensitive to the distribution of an electron cloud. This trend accords well with the results obtained by Hong *et al.*[32] Furthermore, it is found that with increasing incident energy, the capture probabilities tend to converge at a smaller impact parameter gradually and the peak positions will move towards smaller impact parameters. This imply that close collisions are important for higher energy collisions and the electron-capture process is more likely to appear in a relatively low-energy region.

By integration on the electron capture probabilities, one can obtain the electron capture cross sections. In Fig. 6, the present total electron capture cross sections of water dimer collided by protons with different incident energies are exhibited (red ★). To have a better comparison, the experimental results of protons impacting water vapor with an energy of 1 keV to 100 keV[13,16,53,54] and the theoretical data of protons attacking water molecules and liquid water with an incident energy as low as 10 eV are collected in Fig. 6.[27,28] It should be noted that the charge transfer cross section from Mada *et al.*[27] refers to that in configuration (d) because of the excellent agreement with experimental measurements by Lindsay *et al.*,[16] where the energy in the experiment and theory overlaps.

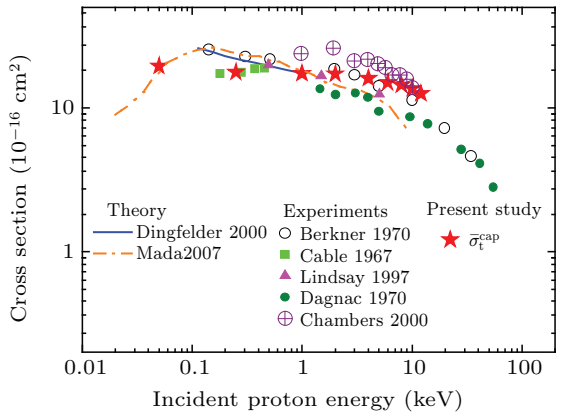


Fig. 6. The total electron capture cross sections $\bar{\sigma}_t^{cap}$ of water dimer as a function of the incident energies (red ★). Various experimental and theoretical results are also provided for comparison. The experimental results are taken from Berkner *et al.*[13] (black ◯), Cable *et al.* (cited by Kooman[12]).[53] (green ■), Lindsay *et al.*[16] (pink ▲), Dagnac *et al.*[54] (olive ●), and Chambers *et al.* (cited by Mada[27]) (purple ⊕). The theoretical results are from Dingfelder *et al.*[28] (blue solid line) and Mada *et al.*[27] (orange dashed dot line).

At first glance, one can see that the electron capture cross sections are relatively abundant when the proton energy ranges from 1 keV to 100 keV corresponding to the energies in which protons tend to have around the Bragg peak. Generally, there are good agreements between the present calculations and available data. At the lowest energy considered, 50 eV, only Mada *et al.*[27] have so far given the theoretical value of the cross section of 50 eV proton colliding with water molecules and our calculated result is in good accord with it. For the energy of 250 eV, the present calculation agrees well with the measurements by Cable *et al.*,[53] but is lower than the measurements by Berker *et al.*[13] For energy of 1 keV, the present result accords well with the calculated results obtained by Mada *et al.*[27] and Dingfelder *et al.*,[28] but is lower than the measurements by Berker *et al.*[13] This discrepancy could be attributed to insufficient consideration of the electron correlation effect since the electron correlation effect becomes more important in low-energy collisions.[55] For energies higher than 1 keV, our results accords well with the measurements by Berker *et al.*[13] and Chambers *et al.*[27] Meanwhile, one can find that the measurements by Dagnac *et al.*[54] are lower than those by Berker *et al.*,[13] implying that a reasonable agreement among all reported measurements is yet to be achieved.

4. Conclusion

In this paper, the fragmentation dynamics of the water dimer under the 50 eV proton impact is investigated theoretically in the the framework of the time-dependent density functional theory, applied to valence electrons, and coupled non-adiabatically to molecular dynamics of ions. The reaction channels, the mass distribution and the fragmentation mass spectrum are explored in six different incident orientations. The reaction channel of PE2 is taken as an example to exhibit the detailed microscopic dynamics of the collision process by inspecting the positions, the respective distance, the number of loss of electrons and the evolution of the electron density. The results show that the different orientations lead to different reaction channels. Among all launched samples, the probability of the channel of NCT and CT is about 80%, hinting that the probability of fragmentation is about 20%. In addition, the probability of the dissociation channel of the O–H DIS2 and the O–H DIS3 is 15.6% and 1.8%, respectively. The study of the mass distribution and the fragmentation mass spectrum shows that among all possible fragments, the fragment with mass 36, i.e., the parent peak, has the highest relative abundance of 65%, followed by the mass 1, which is 20%. Furthermore, the relative abundances of the fragment mass 35 and mass 34 are 13% and 1.5%, respectively. For the total electron capture cross section, the present calculations agree well with the available measurements and calculations over the energy range from 50 eV to 12 keV.

The present work is satisfactory for $H^+ + (H_2O)_2$ collision process. We expect the current results to be predictive even if there is a lack of experimental results for incident energies of less than 1 keV. However, it should be remembered that the temperature effect is not considered in the present study, which

may not be realistic in ambient atmosphere. Work along that direction is in progress.

Acknowledgements

Project supported by the National Natural Science Foundation of China (Grant Nos. 11905160 and 11635003), the '333' project of Jiangsu Province (Grant No. BRA2020327), and the Science Foundation of Wuxi Institute of Technology (Grant No. ZK201903).

References

[1] Bolorizadeh M A and Rudd M E 1996 *Phys. Rev. A* **33** 888
[2] Sobocinski P, Pešić Z D, Hellhammer R, Stolterfoht N, Sulik B, Legendre S and Chesnel J Y 2005 *J. Phys. B: At. Mol. Opt. Phys.* **38** 2495
[3] Gobet F, Eden S, Coupier B, Tabet J, Farizon B, Farizon M, Gaillard M J, Carré M, Ouaskit S, Märk T D and Scheier P 2004 *Phys. Rev. A* **70** 062716
[4] Luna H, Montenegro E C 2005 *Phys. Rev. Lett.* **94** 0043201
[5] Seredyuk B, McCullough R W, Tawara H, Gilbody H B, Bodewits D, Hoekstra R, Tielens A G G M, Sobocinski P, Pesic D, Hellhammer R, Sulik B, Stolterfoht N, Abu-Haija O and Kamber E Y 2005 *Phys. Rev. A* **71** 022705
[6] Jorge A, Horbatsch M and Kirchner T 2020 *Phys. Rev. A* **102** 012808
[7] Gu B, Muñoz-Santiburcio D, Pieve F D, Cleri F, Artacho E and Kohanoff J 2022 *Radiat. Phys. Chem.* **193** 109961
[8] Schardt D, Elsässer T and Schulz-Ertner D 2010 *Rev. Mod. Phys.* **82** 383
[9] Boudaïffa B, Cloutier P, Hunting D, Huels M A and Sanche L 2000 *Science* **287** 1658
[10] Teixeira E S, Uppulury K, Privett A J, Stopera C, McLaurin P M and Morales J A 2018 *Cancers* **10** 136
[11] Nikjoo H, Uehara S, Emfletzoglou D and Brahme A 2008 *New J. Phys.* **10** 075006
[12] Koopman D W 1968 *Phys. Rev.* **166** 57
[13] Berkner K H, Pyle R V and Stearns J W 1970 *Nucl. Fusion* **10** 145
[14] Rudd M E, Goffe T V, DuBois R D and Toburen L H 1985 *Phys. Rev. A* **31** 492
[15] Werner U, Beckord K, Becker J and Lutz H O 1995 *Phys. Rev. Lett.* **74** 1962
[16] Lindsay B G, Sieglaff D R, Smith K A and Stebbings R F 1997 *Phys. Rev. A* **55** 3945
[17] Luna H, de Barros A L F, Wyer J A, Scully S W J, Lecointre J, Garcia P M Y, Sigaud G M, Santos A C F, Senthil V, Shah M B, Latimer C J and Montenegro E C 2007 *Phys. Rev. A* **75** 042711
[18] Tavares A C, Luna H, Wolff W and Montenegro E C 2015 *Phys. Rev. A* **92** 032714
[19] Bernal M A, Liendo J A, Incerti S, Francis Z and Tran H N 2022 *Nucl. Instrum. Methods Phys. Res. Sect. B* **517** 6
[20] Deumens E, Diz A, Longgo R and Öhrn Y 1994 *Rev. Mod. Phys.* **66** 917
[21] Shin W G, Ramos-Mendezd J, Trana N H, Okadae S, Perrotf Y, Villagrasaf C and Incerti S 2021 *Physica Medica* **88** 86
[22] Lekadir H, Abbas I, Champion C and Hanssen J 2009 *Nucl. Instrum. Methods Phys. Res. Sect. B* **267** 1011
[23] Pirkola P and Horbatsch M 2022 *Phys. Rev. A* **105** 032814
[24] Illescas C, Errea L F, Méndez L, Pons B, Rabadán I and Riera A 2011 *Phys. Rev. A* **83** 052704
[25] Lüdde H J, Spranger T, Horbatsch M and Kirchner T 2009 *Phys. Rev. A* **80** 060702
[26] Murakami M, Kirchner T, Horbatsch M and Lüdde H J 2012 *Phys. Rev. A* **85** 052704
[27] Mada S, Hida K N, Kimura M, Pichl L, Liebermann H P, Li Y and Buenker R J 2007 *Phys. Rev. A* **75** 022706
[28] Dingfelder M, Inokuti M and Paretzke H G 2000 *Radiat. Phys. Chem.* **59** 255
[29] Gabás P M M, Errea L F, Méndez L and Rabadán I 2012 *Phys. Rev. A* **85** 012702
[30] Zhao R T, Zhang N and Zhang F S 2018 *Mol. Phys.* **116** 231
[31] Yu W, Gao C Z, Zhang Y, Zhang F S, Hutton R, Zou Y and Wei B 2018 *Phys. Rev. A* **97** 032706
[32] Hong X H, Wang F, Wu Y, Gou B C and Wang J G 2016 *Phys. Rev. A* **93** 062706
[33] Stillinger F H 1980 *Science* **209** 451
[34] Björneholm O, Federmann F, Kakar S and Möller T 1999 *J. Chem. Phys.* **111** 546
[35] See http://www.lpt.ups-tlse.fr/cluster-dynamics/ for the information about the TDDFT-MD model
[36] Dinh P M, Vincendon M, Coppens F, Suraud E and Reinhard P G 2022 *Comput. Phys. Commun.* **270** 108155
[37] Calvayrac F, Reinhard P G, Suraud E and Ullrich C A 2000 *Phys. Rep.* **337** 493
[38] Fennel Th, Meiwes-Broer K H, Tiggesbäumker J, Reinhard P G, Dinh P M and Suraud E 2010 *Rev. Mod. Phys.* **82** 1793
[39] Gao C Z, Wang J, Wang F and Zhang F S 2014 *J. Chem. Phys* **140** 054308
[40] Gao C Z, Wang J and Zhang F S 2013 *Nucl. Instrum. Methods Phys. Res. Sect. B* **307** 225
[41] Wang Z P, Dinh P M, Reinhard P G, Suraud E, Bruny G, Montano C, Feil S, Eden S, Abdoul-Carime H, Farizon B, Farizon M, Ouaskit S and Märk T D 2011 *Int. J. Mass. Spectrom.* **285** 143
[42] Wang Z P, Zhang F S, Xu X F and Qian C Y 2020 *Chin. Phys. B* **29** 023401
[43] Ndongmouo-Taffoti U F, Dinh P M, Reinhard P G, Suraud E and Wang Z P 2010 *Eur. Phys. J. D* **58** 131
[44] Kohn W and Sham L J 1965 *Phys. Rev.* **140** A1133
[45] Marques M A L and Gross E K U 2004 *Annu. Rev. Phys. Chem.* **55** 427
[46] Goedecker S, Teter M and J Hutter 1996 *Phys. Rev. B* **54** 1703
[47] Perdew J P and Wang Y 1992 *Phys. Rev. B* **45** 13244
[48] Legrand C, Suraud E and Reinhard P G 2002 *J. Phys. B* **35** 1115
[49] Ullrich C A 2000 *J. Mol. Struct. (THEOCHEM)* **501–502** 315
[50] Yu W, Zhang Y, Zhang F S, Hutton R, Zou Y, Gao C Z and Wei B 2018 *J. Phys. B: At. Mol. Opt. Phys.* **51** 035204
[51] Wang Z P, Zhang F S, Xu X F, Wang Y B and Qian C Y 2019 *Mod. Phys. Lett. B* **33** 1950257
[52] Rao M V V S, Iga I and Srivastava S K 1995 *J. Geophys. Res.* **100** 26421
[53] Cable P G 1967 *University of Maryland Technical Note* No. BN-499 (unpublished)
[54] Dagnac R, Blanc D and Molina D 1970 *J. Phys. B* **3** 1239
[55] Belkić D, Mančev I and Hanssen J 2008 *Rev. Mod. Phys.* **80** 249